ACS OMEGA

Open Access

http://pubs.acs.org/journal/acsodf

Article

Pharmacophore Model-Based Virtual Screening Workflow for Discovery of Inhibitors Targeting *Plasmodium falciparum* Hsp90

Ofentse Mafethe, Tlhalefo Ntseane, Tendamudzimu Harmfree Dongola, Addmore Shonhai, Njabulo Joyfull Gumede, and Fortunate Mokoena*

Cite This: *ACS Omega* 2023, 8, 38220−38232

Read Online

ACCESS | Metrics & More | Article Recommendations | Supporting Information

ABSTRACT: *Plasmodium falciparum* causes the most lethal and widespread form of malaria. Eradication of malaria remains a priority due to the increasing number of cases of drug resistance. The heat shock protein 90 of *P. falciparum* (PfHsp90) is a validated drug target essential for parasite survival. Most PfHsp90 inhibitors bind at the ATP binding pocket found in its N-terminal domain, abolishing the chaperone's activities, which leads to parasite death. The challenge is that the NTD of PfHsp90 is highly conserved, and its disruption requires selective inhibitors that can act without causing off-target human Hsp90 activities. We endeavored to discover selective inhibitors of PfHsp90 using pharmacophore modeling, virtual screening protocols, induced fit docking (IFD), and cell-based and biochemical assays. The pharmacophore model (DHHRR), composed of one hydrogen bond donor, two hydrophobic groups, and two aromatic rings, was used to mine commercial databases for initial hits, which were rescored to 20 potential hits using IFD. Eight of these compounds displayed moderate to high activity toward *P. falciparum* NF54 (i.e., IC_{50}s ranging from 6.0 to 0.14 μM) and averaged >10 in terms of selectivity indices toward CHO and HepG2 cells. Additionally, four compounds inhibited PfHsp90 with greater selectivity than a known inhibitor, harmine, and bound to PfHsp90 with weak to moderate affinity. Our findings support the use of a pharmacophore model to discover diverse chemical scaffolds such as **FM2**, **FM6**, **F10**, and **F11** exhibiting anti-*Plasmodium* activities and serving as valuable new PfHsp90 inhibitors. Optimization of these hits may enable their development into potent leads for future antimalarial drugs.

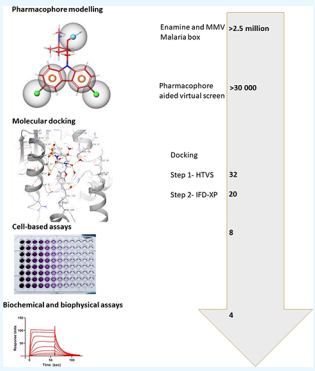

INTRODUCTION

Malaria is responsible for over 619,000 deaths across the globe. Sub-Saharan African populations, especially pregnant women and children under five, disproportionately suffer from the bulk of the disease infection.[1] It has been stated that the disruption of health care services in the recent COVID-19 pandemic could partly contribute to the rising death rates and incidence of malaria.[2] However, there is widespread concern that the recent surge is primarily due to the dissemination of *Plasmodium falciparum* resistant to artemisinin-based combination therapy (ACT).[3,4] Nearly all malaria-endemic populations have reported *P. falciparum*'s resistance to chloroquine.[5,6] Areas such as Rwanda[7] and East Asia[8] have begun to report the presence of *P. falciparum* strains, thus justifying the urgent need to develop potent and reliable antiparasitic drugs. The resistance challenge can be circumvented by urgent identification of chemical compounds less likely to succumb to resistance. Furthermore, *P. falciparum* heat shock protein 90 (PfHsp90) has been implicated in ACT and chloroquine resistance.[9,10]

P. falciparum transitions from a cold-blooded mosquito vector to a warm-blooded human host during its life cycle. Adaptation to the physiologically diverse conditions characterizing life cycle requires the parasite to express a robust molecular chaperone response to help maintain proteostasis.[11] PfHsp90 is one of the most abundant chaperones, which is induced by stress[12,13] and is expressed at all the intra-erythrocyte stages of parasite development.[14] PfHsp90 is critical for the parasite's invasion and survival in the human host.[13] Eukaryotic Hsp90 are large dimeric 90 kDa proteins composed of the N-terminal domain (NTD) that has an ATP binding pocket, the middle domain (MD) for client protein binding, and the C-terminal domain (CTD), serving as a dimerization and tetracopeptide (TPR) containing cochaperone site.[15] Most Hsp90 inhibitors are small molecules competing with ATP to bind the NTD.[16,17] Inhibitor binding traps the Hsp90 in an ADP-bound conformation, consequently blocking the Hsp90 function and precluding client protein maturation.[17] Hsp90 inhibition as a therapeutic strategy has been extensively studied in cancer research, where 17 ATP-competing inhibitors have progressed to different phases of clinical trials. The clinical progression of Hsp90 has often been problematic because of potential off-target and/or Hsp90-

Received: June 23, 2023
Accepted: September 7, 2023
Published: September 26, 2023

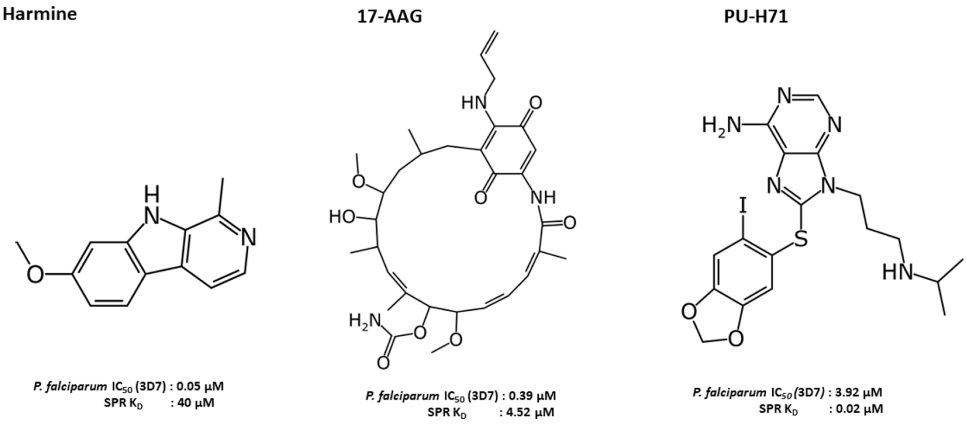

Figure 1. Chemical structures of harmine, 17-AAG, and PU-H71. Parasite growth inhibition values are indicated as well as the binding affinity (K_D) for the respective compounds.

related toxicities due to pan-inhibition.[18,19] However, credence for Hsp90 as a formidable drug target and its selective inhibition was provided by the approval of Pimitespib for treating gastrointestinal stromal tumors (GIST) in Japan with clinical trials being conducted in Europe and America.[20]

PfHsp90 has received some research attention.[13,14,21] However, studies that focused on designing or discovering new compounds inhibiting PfHsp90 are relatively limited compared to human Hsp90.[22−24] Most of the previous studies have repurposed anticancer agents to understand the structure−function of PfHsp90. It was shown that these inhibitors terminate the parasite's growth during both the blood and liver stages.[21,25] Preclinical validation of PfHsp90 as a target for malaria was demonstrated using harmine, 17-AAG, and PU-H71 (see Figure 1 for anti-*Plasmodium* and binding affinity data), and these compounds were shown to clear parasitaemia in *Plasmodium berghei*-infected mice models.[9,21]

The highly conserved nature of the ATP binding region found at the NTD of PfHsp90 (sequence identity >70%) versus human Hsp90 presents a significant challenge regarding the design of inhibitors that are selective toward PfHsp90.[26] However, the availability of the crystal structure of the PfHsp90 bound to ADP has improved the drug discovery landscape in the recent years.[26] Comparison of the ATP and drug binding sites found on PfHsp90 with human Hsp90 uncovered important differences. For instance, the presence of Ile173 in PfHsp90 instead of Val186 in human Hsp90 slightly constricts the posterior end of its binding pocket. The substitution of Ser52 to Ala38 in PfHsp90 has increased the hydrophobicity of the ATP binding pocket.[26] Wang and co-workers proposed that the substitution of Lys112 in human Hsp90 by Arg98 in PfHsp90 affords inhibitor selectivity across species.[27] Furthermore, human Hsp90 homologues possess a glycine-rich loop (GHL) that is more compact due to residues Gly135 and Gly114 being clipped together. In contrast, the GHL in PfHsp90 possesses a straight conformation, disconnecting Gly212 from Gly100 and opening a hydrophobic cavity that can accommodate selective inhibitors.[27] harmine was reported as the first potent and selective inhibitor of PfHsp90 over the human Hsp90.[28] Using surface plasmon resonance and site-directed mutagenesis, it was previously demonstrated that Arg98 was responsible for the selectivity of harmine.[28] In other studies, rational design strategies implementing molecular docking and molecular dynamics simulations were used to identify novel, potent, and selective inhibitors of PfHsp90.[29,30] We used the gains and information from previous studies to develop a pharmacophore model trained using the structures of the selective inhibitors of PfHsp90 obtained from the literature. The hypothesis generated was used to investigate pharmacophores of compounds obtained from commercial databases to enable the identification of selective inhibitors of PfHsp90. These initial hits were rescored by induced fit docking, resulting in 20 potential hits. We identified a few promising hit candidates effective against the *P. falciparum* NF54 cell line and evaluated their *in vitro* on-target effect on purified recombinant PfHsp90 and human Hsp90 to establish selectivity. Therefore, this study reports the rational drug design and the biological *in vitro* evaluation of drug-like molecules as potential inhibitors of PfHsp90.

METHODS

Computational Analysis. The graphical user interface (GUI) of Schrödinger 2021-2,[31] Maestro version 12.9[32] was used for all computational calculations and analyses. Modules such as Phase, Glide, and Induced Fit were used to, respectively, conduct pharmacophore hypothesis generation, hypothesis validation, virtual screening workflow, and induced fit docking, and molecular dynamics simulation. This was thanks to a national license at the Centre for High Performance Computing (CHPC) that is available for Schrödinger software tools installed in Linux servers, in Cape Town, South Africa.

Protein Retrieval and Preparation. The three-dimensional crystal structures of PfHsp90 (PDB ID: 3K60; Chain A, resolution 2.30 Å)[26] and human Hsp90 (PDB ID: 1BYQ resolution 1.50 Å)[33] were downloaded from the protein data bank (PDB) (https://www.rcsb.org/) and prepared using Schrödinger's protein preparation wizard.[31] This involves correcting bond orders, adding hydrogen atoms, creating zero-order bonds to metals, creating disulfide bonds, filling in missing side chains and loops, and deleting water molecules beyond 5 Å to refine the target protein structures.[31] The ionization states of the heteroatoms were measured by Epik at pH 7.4. This was then followed by interactive optimization of altered species in the preprocessing step using PROPKA at pH 7.0, and restrained minimization to obtain the protein in its lowest energy conformation that has converged at an RMSD of 0.30 Å was performed by using an OPLS4 force field.

https://doi.org/10.1021/acsomega.3c04494
ACS Omega 2023, 8, 38220−38232

Ligands Rendering, Retrieval, and Preparation. The 2D structure of each ligand from the literature[29,30] of selective inhibitors of PfHsp90 was drawn using a 2D Sketcher panel in Maestro and conformers generated using a MacroModel module to obtain low-energy 3D structures of the compounds.[34] The database of potential hit compounds was generated by a phase module using Enamine 2015/16 collection (https://Enamine.net/compound-collections/real-compounds/real-database) and Medicine of Malaria ventures (MMV) malaria box databases containing 2.5 million and 400 drug-like compounds, respectively. To ensure high quality and the correct chirality in the 3D structures of the compounds, an LigPrep module on Schrödinger[35] was employed to prepare the ligands. Ionization states for the compounds were generated at a pH of 7.4, and the Epik and tautomeric states were generated followed by the desaltation of ligands. An OPLS4 force field was used for the minimization of the compounds and a maximum of 32 stereoisomers was generated for each ligand.[36]

Pharmacophore Hypothesis Generation and Validation. This study sought to develop a pharmacophore model informed by important chemical features of 31 selective inhibitors of PfHsp90 with anti-*Plasmodium* activity obtained from the literature.[29,30] These IC_{50} values of the compounds ranging from 70 to 18,000 nM (Table S1) were converted pIC_{50} (Table S1) for normalization of the data using an online tool (http://www.sanjeevslab.org/tools.html). The 2D structure of each compound was drawn using 2D Sketcher on Maestro and optimized to low-energy 3D conformation using MacroModel.[34] The pharmacophore model was created by using a subset of multiple ligands from Wang et al.[29] and Everson et al.[30] The active and inactive sets were defined by using experimental pIC_{50} from literature.[29,30] Furthermore, the activity threshold for the actives was set at a pIC_{50} of $\geq$7.00, while the threshold for the inactives was set at a pIC_{50} of $\leq$5.70. Therefore, a total of four compounds were actives and a total of 24 compounds were inactives. The most active compounds that were used to generate the pharmacophore model were compounds **5B**, **2D**, **5E**, and **5A** (Table S1). Default settings were used to generate 10 conformations per rotatable bond, resulting in a total of 50 conformers. A total of 20 hypotheses were generated and ranked based on several statistical metrics, which include vector, volume, site, and survival scores. Hypothesis was validated by taking the 31 compounds from literature[29,30] that were used to develop the model and compounds from the DUD database as a subset of decoys. The validation of the model was used to assess the ability of the generated hypothesis to differentiate between active and decoy compounds[37] and provide a quality estimation of the hypothesis. Active compounds are recognized selective inhibitors of PfHsp90, whereas decoy molecules show no activity toward PfHsp90. The DUD-E decoy set of a subset of 58 compounds was uploaded from a Phase pharmacophore tutorial (https://content.schrodinger.com/tutorials zipfile/2022−1/lbvs_phase_ligand.zip). Some statistical parameters such as the enrichment factor (EF), BEDROC, receiver operating characteristics, and area under curve (ROC-AUC), which measure the performance of the hypothesis by distinguishing between active and inactive compounds, were measured.[38]

Phase Database Generation and Database Screening. A subset of compounds from Enamine and MMV databases was used to generate a database of potential hit compounds for this study. First, a library of compounds was prefiltered using Lipinski's rule of 5. This entails compounds that meet the following criteria: molecular weight $\leq$500 g/mol, hydrogen bond donors $\leq$5, hydrogen bond acceptors <10, and cLoP (lipophilicity) <5[38,39] were screened using Qikprop. Second, the drug-like compounds that survived the screen were then desalted and neutralized at a physiological pH of 7.4 using Epik and the OPLS4 force field was used to minimize the resulting conformers. The validated pharmacophore model was then used to screen the Enamine and MMV databases of drug-like compounds to obtain initial hit compounds through the Phase module.[37] These initial hits were analyzed by aligning them to the generated hypothesis. The calculation of key parameters such as the fitness score, site score, vector score, volume score, and alignment score was used to determine the precision of the match between the database compounds and the hypothesis.

Virtual Screening Workflow. The virtual screening workflow (VSW) using Glide[40] was conducted to filter potential hits of compounds from the databases. The idea is to place the ligand in the ATP binding pocket of PfHsp90. We also assessed the selectivity of the screened compounds by binding them to human Hsp90 in the VSW. In the VSW, all screening compounds were subjected to Qikprop to measure their physicochemical and ADME properties. This was followed by the removal of compounds with reactive functional groups. Subsequently, the receptor grids for both hHsp90 and PfHsp90 were generated prior to high-throughput virtual screening (HTVS) using Glide.[40] The cocrystallized ligands were used for positional constraints. Residues such as Asn37, Arg98, and Phe124 found in the ATP binding pocket of PfHsp90 were used to generate hydrogen bond constraints. First, the ligand structures were sequentially docked into the target grid in HTVS mode. The docking step was parametrized as the top 10% of the best compounds to be retained in Glide-HTVS. Second, Glide docking using the standard precision (SP) mode was used. Finally, the top 10% of the best compounds were subjected to the Glide extra-precision (XP) mode docking step. Docking poses that survived this docking step were further analyzed and selected using visual inspection and docking scores.

Induced Fit Docking and Free Binding Energy Calculations. The induced fit docking (IFD) procedure accounts for the flexibility of both the ligand and receptor during docking. Meanwhile, the VSW only accounts for the flexibility of the ligand and some amino acids in the receptor in the active site, whereas the entire receptor conformation is held rigid during docking. As such, an IFD was employed to further screen the compounds against PfHSP90 using a method that accounts for induced fit effects. A protocol previously described in the literature[41] using IFD was employed using Glide.[40] The hits obtained from the virtual screening workflow were docked to the rigid protein using Glide with a van der Waals (vdW) radius scaling of 0.5 Å for the protein and ligand nonpolar atoms. Energy minimization was carried out on the PfHsp90 and human Hsp90[26] protein structures using the force field OPLS4 with an implicit solvation model. The Glide XP mode was utilized for the initial docking using zinc as the metal constraint atom, and 20 ligand poses were retained for protein structural refinement. The prime module[42] was used to develop the induced fit protein−ligand complexes. Each of the 20 structures from the previous step was subjected to side chain and backbone refinements. All the residues with at least one atom located within 5.0 Å of each

https://doi.org/10.1021/acsomega.3c04494
ACS Omega 2023, 8, 38220−38232

corresponding ligand pose were included in the prime refinement. The refined complexes were ranked by prime energy, and the protein structures within 30 kcal/mol for the minimum energy structure were put through the final round of Glide docking and scoring. Each ligand was redocked into every refined low-energy protein structure by using Glide XP.

Additionally, the free binding energy of the best docked GlideXP poses of PfHsp90 and ligand complexes was calculated using the OPLS_2005 force field and rotamer algorithm within the molecular mechanics with generalized born surface area (MM/GBSA)-prime module of Schrödinger.[43] The free binding energy equation used was

$$\Delta G\text{binding} = \Delta G(\text{complex}) - \Delta G(\text{protein}) - \Delta G(\text{ligand}) \quad (1)$$

Cell-Based Assays. *In Vitro Anti-Plasmodial Assay.* Triplicates of all 20 potential hit compounds were evaluated for anti-*Plasmodial* activity using a parasite lactate dehydrogenase assay as a marker for parasite survival on two separate occasions. Briefly, the respective stock solutions of reference drugs, chloroquine (CQ) and artesunate (ART), and 10 mM DMSO (100%) for test compounds were then stored at −20 °C. Further dilutions were prepared on the day of the experiment. To evaluate anti-*Plasmodium* activity against *P. falciparum* NF54 parasites, continuous *in vitro* cultures of asexual erythrocyte stages of *P. falciparum* were maintained using a modified protocol of ref 44. Parasite cultures were synchronized to the ring stage using 15 mL of 5% (w/v) D-sorbitol in water. Synchronous cultures of *P. falciparum* NF54 in the ring stage were prepared for 2% parasitemia and 2% hematocrit. Compounds were tested at starting concentrations of 6000 nM (300 nM for CQ), which were then serially diluted 2-fold in a complete medium to give 10 concentrations with a final volume of 200 μL in each well. Parasites were incubated in the presence of the compounds at 37 °C under hypoxic conditions (4% CO_2 and 3% O_2 in N_2) for 72 h. After incubation, 100 μL of the MalStat reagent and 15 μL of the resuspended culture were combined followed by the addition of 25 μL of nitro blue tetrazolium chloride. The plates were kept in the dark for 10 min to fully develop, after which the absorbance was measured at 620 nm on a microplate reader. Raw data were processed using GraphPad Prism 9.0 (La Jolla, California, USA) to analyze the dose−response data.

In Vitro Cytotoxicity. All 20 potential hit compounds were screened for *in vitro* cytotoxicity against mammalian cells Chinese Hamster Ovarian (CHO) and hepatocellular carcinoma (HepG2) using the 3-(4,5-dimethylthiazol-2-yl)-2,5-diphenyltetrazolium bromide (MTT) assay.[45] Test compounds were prepared with the highest concentration of solvent to which the cells were exposed, having no measurable effect on the cell viability (data not shown). The initial concentration of the compounds and control was 50 μM, which was serially diluted in a complete medium with 10-fold dilutions to give six concentrations, the lowest being 0.09 μM. Emetine (50 μM) was used as a positive control compound for cytotoxicity assessment and DMSO as negative control wells. The 50% inhibitory concentration (IC_{50}) values were obtained from full dose−response curves using a nonlinear dose−response curve fitting analysis via GraphPad Prism 9.0 software.

Biochemical Analysis. *Materials.* Unless otherwise stated, all of the chemicals and solvents utilized were purchased from Sigma-Aldrich Co., Ltd. (Steinheim, Germany) and Thermo Fisher Scientific (Illinois, USA).

Competition Binding Assays. Protein expressions and purifications of the N-terminal domains of PfHsp90 (residues 1−215, PlasmoDB ID PF3D7_0708400) and human Hsp90β (residues 1−226, Uniprot: P08238) were conducted using a modified protocol.[46] All compounds exhibiting antimalarial activity were assessed for their ability to displace fluorescein isothiocynate (FITC)-geldanamycin (GDA) from PfHsp90-NTD and human Hsp90β-NTD by the fluorescence polarization assay (FPA) following a protocol developed in ref 25. Briefly, the FPA buffer (20 mM HEPES, pH 7.4, 50 mM KCl, 5 mM $MgCl_2$, 20 mM Na_2MoO_4, 2 mM DTT, 0.1 mg/mL bovine growth globulin, 0.01% Triton-X) was prepared and mixed with 5 nM of FITC-GDA. In a black 96-well plate, the mixture prepared was added together with PfHsp90-NTD and human Hsp90β-NTD at a final concentration of 100 nM to a total reaction volume of 50 μL. Test compounds at 10 μM, known inhibitors of PfHsp90, harmine, and PUH-71, were used as positive controls, and a final concentration of 1% DMSO was used for reaction. FITC-GDA without the chaperone and with the chaperone bound to FITC-GDA were used as negative and positive controls, respectively. Plates were incubated with shaking overnight at 4 °C. The FP signal was measured using a 480 nm excitation filter and a 535 nm emission filter in the Glomax Explora spectrometer system. The FP signal was converted to percent bound FITC-GDA based on the DMSO control and plotted using GraphPad Prism 9.0.

ATPase Assay. All compounds exhibiting antimalarial activity were studied for their capabilities of disrupting the ATPase activity of PfHsp90 by following the previously described protocol.[21,47] The assay monitors the amount of inorganic phosphate released as an indication of the chaperone's ability to hydrolyze ATP. Briefly, 2 μM PfHsp90-NTD and human Hsp90β-NTD in the assay buffer (0.5 M HEPES pH 7.4, 0.5 M MgCl2, 0.5 M KCl, and 10 mM dithiothreitol (DTT)) were incubated in the absence and presence of varying compound concentrations of study compounds. The reaction was initiated by addition of 1 mM ATP followed by incubation for 30 min at room temperature. Subsequently, 10% SDS was added to terminate the reaction. Serving as positive control, harmine was used, and as negative controls, BSA and boiled PfHsp90-NTD were used. The reaction was developed by addition of 1% ammonium molybdate and 6% ascorbic acid and the released inorganic phosphate (measured as Pi released/min/mg protein) and quantified using a Glomax explorer spectrometer (Promega, USA) at an absorbance of 660 nm.

Determination of Equilibrium Binding Kinetics. The direct interaction of selected study compounds with PfHsp90-NTD was investigated using multiparametric surface plasmon resonance (MP-SPR, BioNavis, Finland) as previously described in refs 48 and 49. In brief, filter-sterilized degassed PBS (4.3 mM Na_2HPO_4, 1.4 mM KH_2PO_4, 137 mM NaCl, 3 mM KCl, 0.005% (v/v) Tween 20, and 20 mM EDTA; pH 7.4) was used as running buffer for the assay. PfHsp90-NTD (20 μg/mL) serving as a ligand was immobilized through amine coupling onto a carboxymethyl dextran (CMD 3-D) gold sensor, and compounds (0−2000/5000 nM) were injected at a flow rate of 50 μL/min as the analyte. Positive controls including known inhibitors of PfHsp90, GDA, and harmine were similarly injected at varying final concentrations

https://doi.org/10.1021/acsomega.3c04494
ACS Omega 2023, 8, 38220−38232

of 2000 nM over the chip surface. A reference channel without immobilized protein served as the control for nonspecific binding and changes in the refractive index. Association and dissociation were monitored for 1 and 9 min, respectively, at room temperature. The data generated were analyzed after subtraction of the baseline (signals generated on the chip surface without the protein immobilized and buffer without the inhibitor) using a Data Viewer (BioNavis, Finland).

RESULTS AND DISCUSSION

Generation of a Ligand-Based Pharmacophore Model. In our effort to identify new chemical scaffolds from the Enamine and MMV malaria box databases with a high probability of binding to PfHsp90 and inhibiting *P. falciparum* growth, a combination of structure-based (docking) and ligand-based (pharmacophore modeling) drug design methods was implemented.

Table S1 shows the structures of 31 selective inhibitors of PfHsp90 obtained from the literature,[29,30] which were used to generate pharmacophore models. The compounds were classified as actives (i.e., $pIC_{50} \geq 7.0$) and inactives ($pIC_{50} \leq 5.7$). A total of four active sets of compounds were used to generate 20 pharmacophore models. However, only four pharmacophore models were selected for further studies based on their good vector, volume, site, and survival scores (see Table 1). Pharmacophore hypothesis with features such as

Table 1. Top-Scoring Hypothesis Generated from Pharmacophore Modeling

hypothesis	vector score	volume score	site score	survival score
DHHRR_1	1.000	0.805	0.972	5.507
DHHRR_2	1.000	0.797	0.972	5.498
DHHRR_3	1.000	0.805	0.972	5.492
DHHRR_4	1.000	0.794	0.972	5.484

DHHRR_1 was the highest scoring pharmacophore model with a vector score of 1.00, volume score of 0.805, site score 0.972, and survival score of 5.507 (Table 1). In this pharmacophore model, point vectors are aligned to functional groups of the most active compound **5E** in the training set, and based on this alignment, a vector ranging from 0 to 1 is assigned. A score of 0 indicates poor alignment, while a vector score of 1 indicates a good overlay.[50] The site score, on the other hand, evaluates the fit of the ligand within the protein's binding site and ranges from −1 to 1. The DHHRR_1 hypothesis had a site score of 0.972, suggesting that the ligand fits well with the pharmacophore model, in the absence of a receptor. The stability of the protein−ligand complexes is evaluated by the survival score. A higher survival score indicates that the complex is more stable and less likely to dissociate. Thus, the DHHRR_1 hypothesis demonstrated that the protein−ligand complex is likely to be stable over time as it attained the highest survival score.

The DHHRR_1 hypothesis consisted of five features, namely, one hydrogen bond donor (D), two hydrophobic groups (H), and two aromatic rings (R), as depicted in Figure 2A, which were identified as essential features for inhibitors binding to the ATP pocket of PfHsp90. The strength of the DHHRR_1 pharmacophore model was demonstrated by its overlay to compound **5E** (the active compound in the training set with an anti-*Plasmodial* IC_{50} of 70 nM; Figure 2B). These five features were perfectly overlaid with compound **5E**, while only two features were matched with the least active compound CP-1E, with an IC_{50} of 18,600 nM (Figure 1C). Importantly, there was a lack of alignment between compound CP-1E and the DHHRR_1 hypothesis (Figure 2C). This suggests that the DHHRR_1 hypothesis would be a good and reliable pharmacophore model for identifying inhibitors of PfHsp90.

Hypothesis Validation. The DHHRR_1 pharmacophore hypothesis was validated with the goal of confirming its ability to distinguish between active and inactive compounds. The accuracy of prediction is measured by the area under curve (AUC), with higher AUC values indicating higher accuracy rates.[51] The AUC value ranges between 0 and 1; therefore, by achieving the AUC of 0.61, the DHHRR_1 model demonstrated its capability in distinguishing between active and inactive compounds (Figure 3). Additionally, the receiver operating characteristic (ROC) curve illustrated the sensitivity−specificity relationship.[51] The ROC curve demonstrated a value of 0.39 for DHHRR_1 (Figure 3), suggesting its ability to accurately identify true positives while minimizing false positives. Although the ROC value appears low, it is important

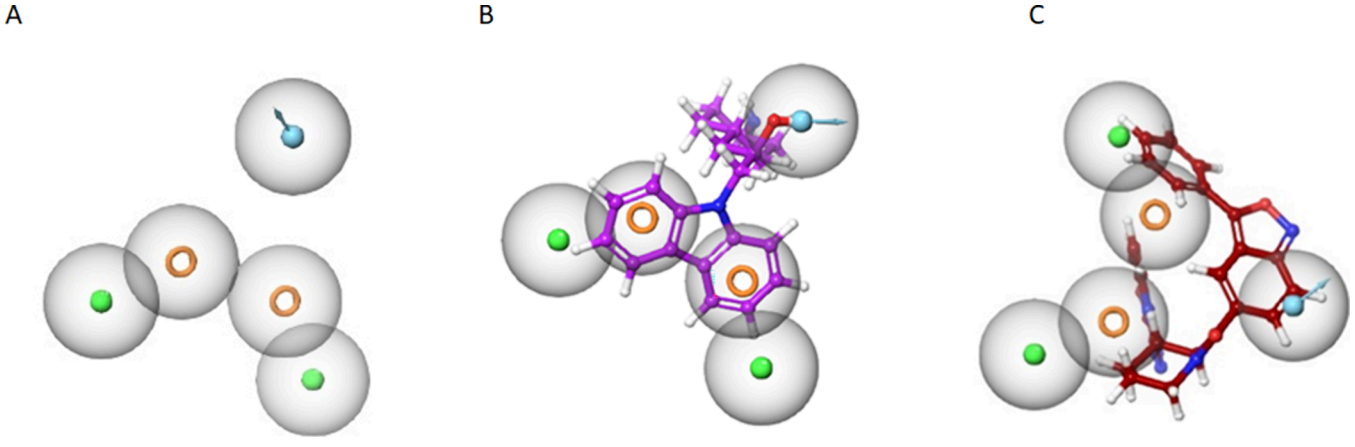

Figure 2. (A) DHHRR_1 pharmacophore hypothesis created using 31 compounds with selective inhibition toward PfHsp90 showing one hydrogen donor (blue), two hydrophobic groups (green), and two aromatic rings (orange). (B) DHHRR_1 pharmacophore hypothesis showing a great alignment with one of the active compounds **5E** (purple). (C) DHHRR_1 pharmacophore hypothesis superimposed to inactive compound CP-1E (maroon).

https://doi.org/10.1021/acsomega.3c04494
ACS Omega 2023, 8, 38220−38232

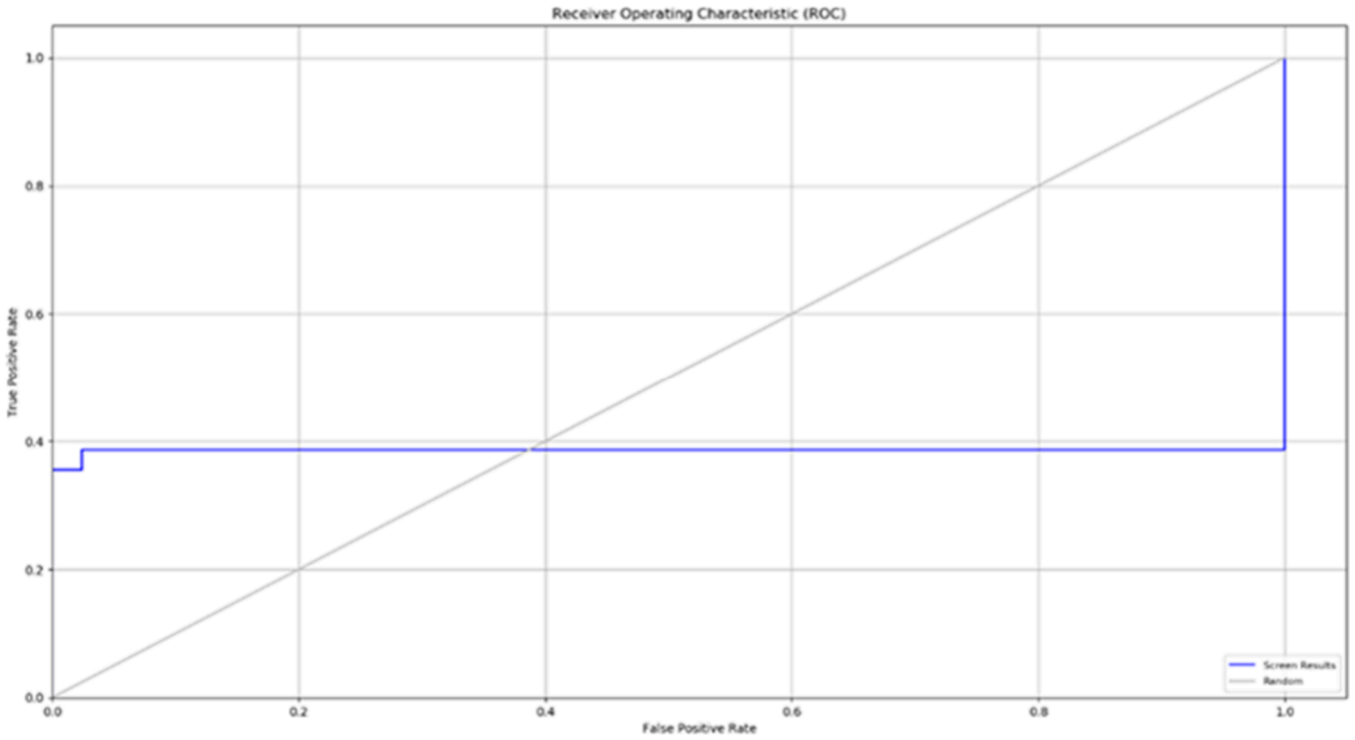

Figure 3. ROC curve obtained by the DHHRR_1 hypothesis, which had a true positive rate of 0.39. The ROC graph of DHHRR_1 hypothesis plotted between the true positive (*Y* axis) and false positive rate (*X* axis). The ROC value of DHHRR_1 is 0.39 that represents the reproducibility and reliability of the model. The blue line represents the performance of the model when it is applied to the screening results, and it is created by varying the threshold value for the predicted scores and plotting the true positive rate (sensitivity) against the false positive rate (specificity). The gray scatter line represents the performance of the model when it is applied to randomly selected instances.

to note the complexity and difficulty of the database screening. Furthermore, the pharmacophore hypothesis was developed by using a subset of 31 active compounds and a decoy set of 58 compounds. Therefore, an enrichment of 40% of actives is satisfactory considering the data used in validating the model. For correct classification of compounds, the enrichment factor (EF) and RIE were also calculated.[51]

Given the inherent difficulty in discovering active compounds from a larger database, the ROC score of DHHRR_1 emphasizes its potential utility within this context. The discriminatory power of the DHHRR_1 hypothesis was demonstrated to be robust by other statistical metrics for hypothesis validation. For example, DHHRR_1 displayed a more robust initial enhancement (RIE) value of 2.26, which further reinforces the model's capacity to enhance the initial hit rate during screening, reducing the chances of missing potential active compounds. Based on the statistical metrics used, it was then believed that the DHHRR_1 hypothesis has greater sensitivity and specificity than other generated hypotheses (DHHRR_2, DHHRR_3, and DHHRR_4). Meanwhile, the need for further refinements of the pharmacophore and validation is acknowledged. The study suggests that the DHHRR_1 model is a valuable tool for database screening in antimalarial drug discovery. The combination of its enhanced performance metrics, including AUC, ROC, RIE, and EF values, highlights its potential to be reliable for discovering novel inhibitors of PfHsp90.

Pharmacophore Model-Aided Virtual Screening. The DHHRR_1 hypothesis was used to search the Enamine and MMV malaria box databases, which contained 2.5 million and 400 drug-like compounds, respectively. The primary goal of this screening was to discover chemically diverse novel inhibitors of PfHsp90. The screening criteria for these possible hits were as follows: first, selecting compounds with a fitness score greater than 1.5. Second, to select compounds that matched the DHHRR_1 hypothesis (i.e., compounds that demonstrated excellent alignment when superimposed with the DHHRR_1 hypothesis). One reason for selecting hits with perfect alignment to the DHHRR_1 model is to avoid the possibility of selecting hits with an acceptable 3D arrangement of functional groups but the improper shape or size, which could prohibit it from fitting into the target's binding site. The DHHRR_1 hypothesis was scanned against the Enamine database yielding 33,214 and MMV malaria box yielding 75 initial hits from each of the database, which were then subjected to a virtual screening approach to assess their ability to bind to the PfHsp90 pocket. The initial hits were used as input hits for high-throughput virtual screening (HTVS) during the virtual screening workflow (VSW), and 10% of the best output hits were subjected to a faster and less computationally intensive standard precision (SP) method that overlooks important conformations of the protein−ligand complex. Finally, extra-precision (XP) docking was performed using 10% of the best SP output, which utilizes more exhaustive search algorithms that thoroughly explore the conformational space, increasing the likelihood of finding the correct binding mode. Docking scores and visual inspection were used as criteria to determine the binding affinity of the screened subset of compounds. A total of 20 initial hits as potential PfHsp90 inhibitors were selected for further screening (Figure S1).

https://doi.org/10.1021/acsomega.3c04494
ACS Omega 2023, 8, 38220−38232

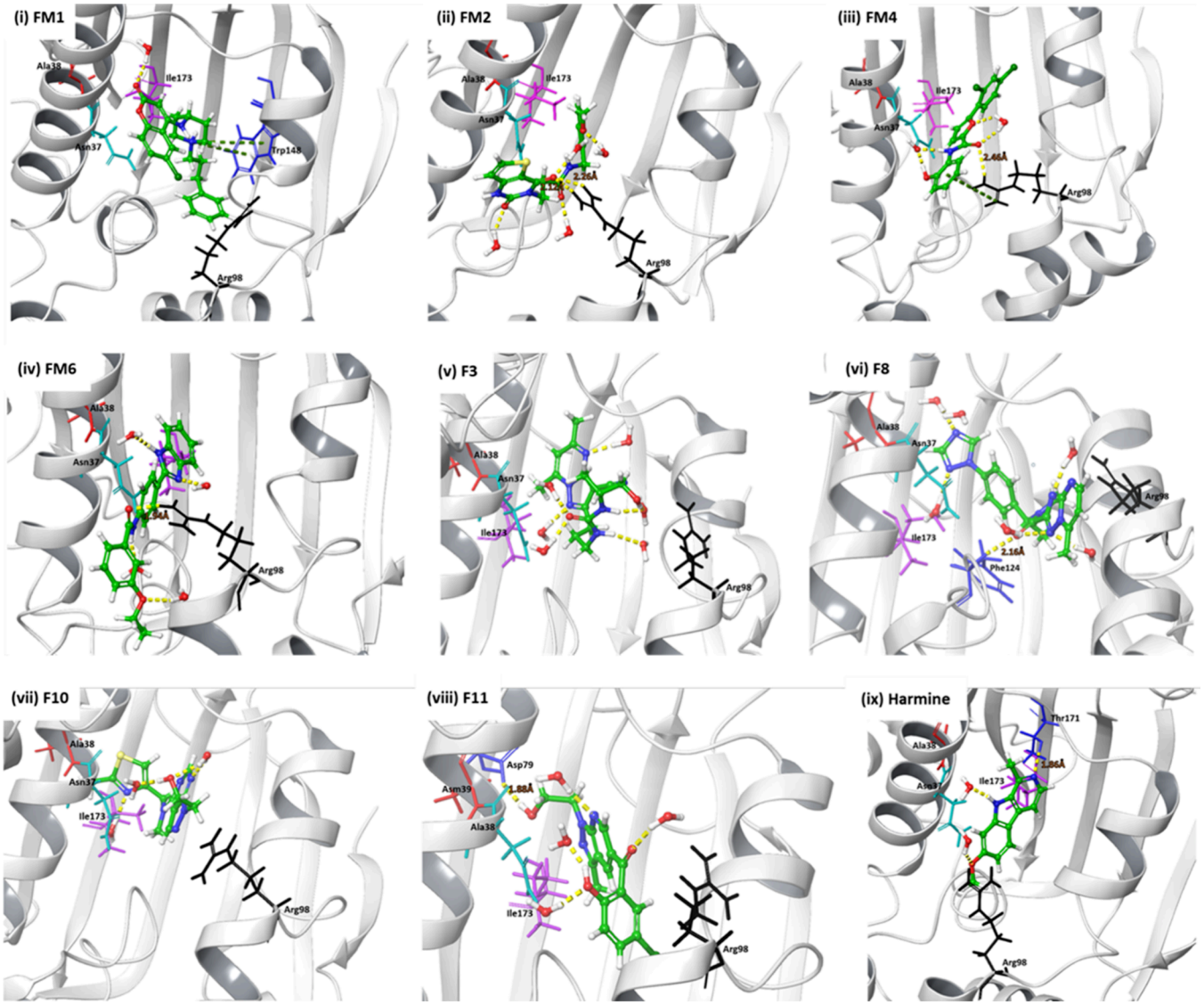

Figure 4. IFD poses of the compounds in the active site cavity of PfHsp90. Candidate compounds showing carbon atoms colored in green, oxygen atoms in red, and nitrogen atoms in blue are the residues interacting with the compounds. The amino acids unique to PfHsp90 are colored in red, black, and purple for residues Ala38, Arg98, and Ile173, respectively. Other important ATP binding residues, including Asn37 (annotated in cyan) and Asp79 (annotated in blue), are also shown. Yellow dashes are the hydrogen bonds, and green dashes indicate $\pi-\pi$ and πpi-cation interactions. Written in orange are the bond radii measured in Angstroms (Å).

Cross-Docking. The cross-docking procedure was performed to assess the accuracy of the Glide docking protocol for PfHsp90 and hHsp90. The main idea was to reproduce the binding conformations of ADP to PfHsp90 as well as GTP to human Hsp90, respectively, since the accuracy of docking scoring functions is system-dependent. As such, the cross-docking poses of ADP to PfHsp90 revealed a root-mean-square deviation (RMSD) of 0.2 Å and a docking score of −14.497 kcal/mol. The native binding conformation of ADP to PfHsp90 was successfully reproduced (Figure S2). Hydrogen bonds between ADP and PfHsp90 such as Asp79 with a bond radius of 2.44 Å, Asn37 with bond radii of 1.98 Å, and Arg98 with bond radii of 1.63 and 2.29 Å are shown (Figure S2). The cross-docking suggested that endogenous compound ADP-PfHsp90 recognition is influenced by the hydrogen bonds with Asp79, Asn37, and Arg98. Therefore, these observations validate the conclusion made by Wang et al.[27] that the binding of drugs to Arg 98 in the ATP binding site of PfHsp90 are important for their anti-*Plasmodium* activities. It was interesting to note that the cross-docking of GTP to human Hsp90 did not reproduce the native binding conformation of GTP to hHsp90. Instead, the diphosphate moieties are superimposed, while the 2-amino-5,7-dihydro-6*H*-purin-6-one moieties are not superimposed (Figure S3). In fact, they have adopted different binding modes, which means that docking did not capture the native binding conformation of GTP to hHsp90. An RMSD of 4 Å further confirms this nonalignment of the cross-docking pose and the X-ray crystal structure's conformation. This then proves that the accuracy of docking algorithms is system-dependent.[55−60]

Induced Fit Docking. IFD was used to estimate the binding mode and binding affinities of the candidate compounds to PfHsp90 and human Hsp90. The IFD process grants flexibility to the side chains of the protein, enabling the ligand to adapt and improve its binding interactions within the binding site. The evaluation of the 20 potential hit candidates

https://doi.org/10.1021/acsomega.3c04494
ACS Omega 2023, 8, 38220−38232

Table 2. Hits Obtained from the Virtual Screening Were Subjected to Induce Fit Docking against PfHsp90[a]

compound	docking score	IFD score	ΔGBind	ΔGBind Coulomb	ΔGBind Covalent	ΔGBind Hbond	ΔGBind Lipo	ΔGBind Packing	ΔGBind vdW
FM1	−10.7	−521	−63.1	−39.6	2.0	−5.7	−5.9	−1.6	−41.7
FM2	−9.1	−520	−53.1	−29.6	2.0	−5.7	−5.9	−1.6	−41.7
FM4	−7.2	−515	−44.1	−17.5	8.8	−7.8	−6.3	−0.5	−33.4
FM6	−6.8	−516	−25.1	−31.7	6.6	−3.3	−8.5	−3.0	−24.3
F3	−10.9	−521	−40.9	−29.5	3.1	−4.6	−6.1	−0.5	−29.7
F8	−11.0	−517	−41.6	−35.7	5.6	−5.4	−6.0	−1.4	−24.2
F10	−7.2	−525	−18.2	−39.8	2.3	−3.7	−3.2	−1.5	−27.5
F11	−10.8	−524	−16.9	−13.7	5.0	−3.9	−5.6	−3.0	−26.9
5E	−10.1	−508	−28.4	−16.4	4.2	−3.7	−7.6	−4.0	−34.1
harmine	−6.8	−517	−27.5	−3.2	1.7	−1.7	−11.2	−2.7	−28.8

[a]Compounds with their corresponding XP Gs docking scores and IFD scores in kcal/mol as well as their predicted MM-GBSA binding free energies (kcal/mol). ΔGBind Coulomb: coulomb energy, ΔGBind Covalent: covalent binding, ΔGBind Hbond: hydrogen bonding, ΔGBind Lipo: the lipophilic binding binding, ΔGBind Packing: $\pi-\pi$ packing intaractions, and ΔGBind vdW: the van der Waals energy (vdW).

targeting PfHsp90 reveals that their relative binding affinity estimates represented by the docking scores fall within a range of −7.2 to −11.0 kcal/mol (Table 2). Most of the hit compounds demonstrated affinities similar to those of known and proven inhibitors of PfHsp90, such as harmine (−6.8 kcal/mol) and compound **5E** (−10.1 kcal/mol). Compounds **F3**, **5E**, **F8**, **F11**, and **FM1** exhibited docking scores greater than or equal to −10 kcal/mol (Table 2). The knowledge of the binding mode of endogenous compound ADP to PfHsp90 estimated by using cross-docking helped us to set up a criterion to be used for visual inspection of candidate compounds.

The prime MM-GBSA module within the Prime Schrödinger suite was used to calculate the binding free energy of the docked complexes. The relative free binding energies of **FM1**, **FM2**, and **FM4** were −63.1, −53.1, and −44.1 kcal/mol, respectively, which were higher than proven inhibitors harmine and compound **5E**. Compound **FM6** exhibited comparable relative free binding energy to control known inhibitors (Table 2)

To select the best pose from among the 20 compounds, various factors were considered, including the docking score, IFD score, and visual inspection of the binding orientation. It was previously reported that harmine is selective toward PfHsp90 through water-mediated interaction with Arg98.[28] As such, binding of compounds **FM2**, **FM4**, and **FM6** to Arg98 through direct hydrogen bonding (Figure 5) plays a major role in the potency of these compounds to PfHsp90. The hydrogen bond between **FM2**, **FM4**, **FM6**, and Arg98 is important in the anti-*Plasmodial* recognition of the candidate compounds, as evidenced by the hydrogen bond between ADP and Arg98 of PfHsp90 (Figure S1). Furthermore, **FM2** exhibits hydrogen bonds with Arg98 with bond radii of 2.12 and 2.26 Å, respectively. Phe124 further hydrogen bonds with **FM2** with a bond radius of 1.80 Å. **FM6**, on the other hand, has exhibited a $\pi-\pi$ interaction with Arg98, and **FM6** also hydrogen bonds with Phe124 with a bond radius of 1.94 Å (Figure 4). This indicates strong binding between **FM6** and PfHsp90. The binding mode of the top scoring hit compounds was consistent with other potential hit compounds (Figure S4). Interestingly, with the exception of **FM2**, most of the top scoring and other candidate hit compounds did not interact with Lys112 when docked to human Hsp90 (Figures S5 and S6)

Anti-*Plasmodial* and Cytotoxicity of Promising Compounds. The 20 compounds were tested *in vitro* for anti-*Plasmodial* activity and profiled for cytotoxicity against the CHO and HepG2 cell lines, with a total of eight compounds showing promising anti-*Plasmodial* activity (PfNF54 IC_{50} < 6 μM) and the remaining compounds being inactive (IC_{50} > 6 μM) (Table S3). The most active compound was **FM2** (PfNF54 IC_{50}: 0.14 μM) exerting ideal selectivity indices (SI > 357) toward both CHO and HepG2 cells (Table 3). While **FM4** demonstrated submolar potency toward *P. falciparum,* it was found to be toxic HepG2 cells. Due to its lack of selectivity against HepG2 cells, compound **FM5** was excluded from further analysis. Overall, seven compounds demonstrated promising anti-*Plasmodium* activity, though compounds **F11**, **FM4**, and **FM6** would need to be optimized for their selectivity against HepG2 cells.

Binding Assays. We evaluated the inhibitory activity of eight study compounds that exhibited anti-*Plasmodium* activity against PfHsp90 and human Hsp90. We purified each chaperone by nickel affinity chromatography from *Escherichia coli* T7 cells (Figure S7) and incubated them with fluorescein isothiocyanate (FITC) tagged to GDA. Reduction of the amount of FITC-GDA bound to PfHsp90/human Hsp90 after the compound's introduction was converted to % inhibition. Compounds **F10** and **F11** showed potent inhibitions of 97 and 93%, respectively, while the compound showed a moderate inhibition of 48% (Table 4 and Figure S8). The three compounds inhibit PfHsp90 more effectively than harmine at 7% inhibition using 10 μM. Compounds **FM1**, **F10**, and **F11** were also shown to inhibit human Hsp90, although not as effectively as PfHsp90, at 23, 44, and 38%, respectively (Table 4 and Figure S8). Compounds **FM2**, **FM4**, and **FM6** could be regarded as selective since they did not inhibit human Hsp90 (Table 4 and Figure S8), with **FM2** showing moderate inhibition of PfHsp90 at 69%. Overall, the data obtained suggested that the candidate hit compounds could serve as a starting point for drug discovery based on their selectivity toward PfHsp90.

SPR was used to determine the binding affinity constant, K_D, which is calculated by dividing the K_d/Ka, where Ka represents the association constant, which is signaled by an increase in response and K_d represents the dissociation rate that is signaled by a decrease in the RU signal. The binding affinity data obtained are summarized in Table 4. In general, study compounds were found to have a lower binding affinity within the submolar range representing tighter binding than harmine (Table 4). Compounds **FM4** and **F11** bound with moderate affinity to PfHsp90 within the same order of magnitude as harmine and GDA, while compound **FM2** bound with weak affinity.

https://doi.org/10.1021/acsomega.3c04494
ACS Omega 2023, 8, 38220−38232

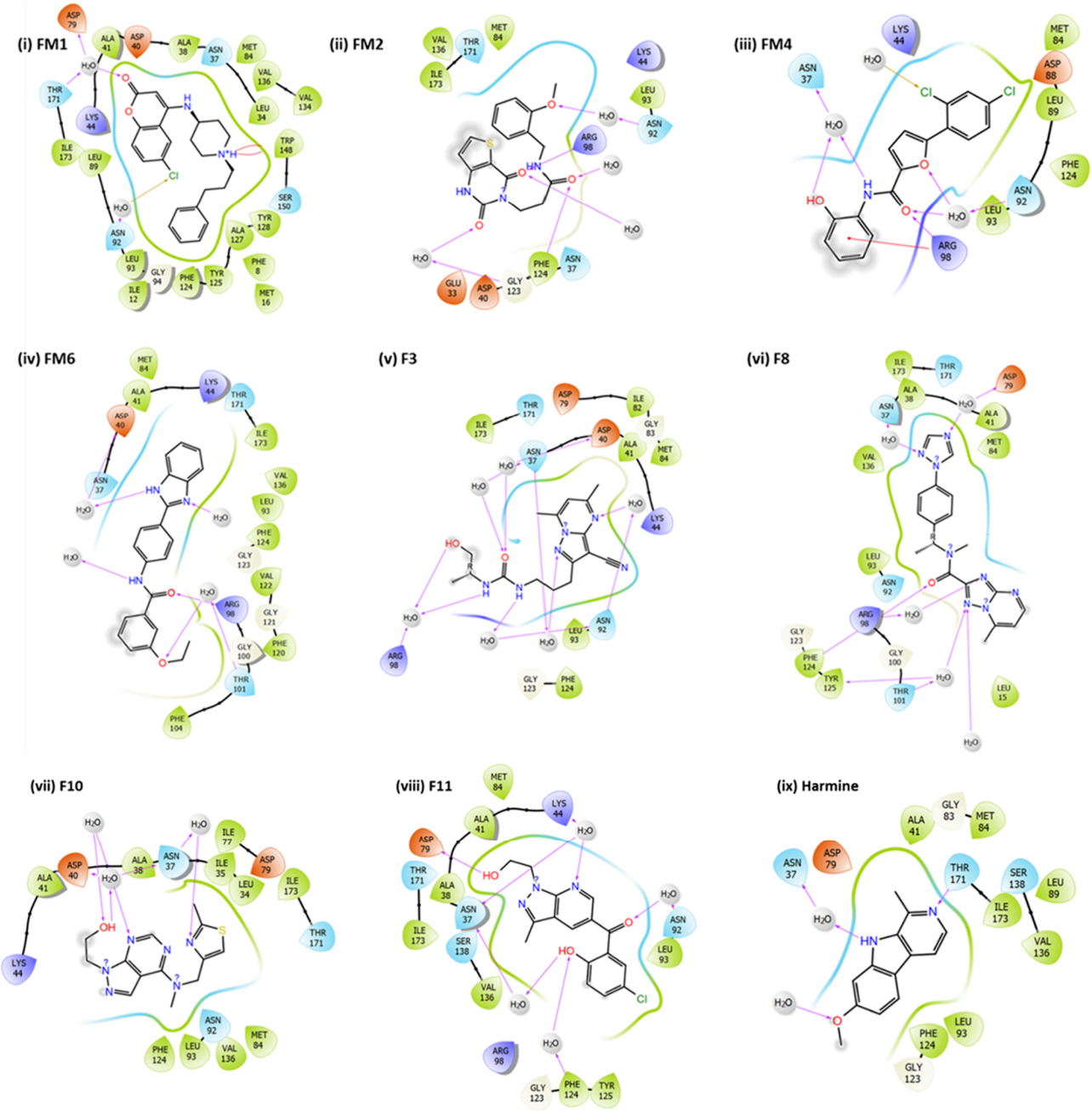

Figure 5. 2D ligand interaction diagrams for the respective compounds. Positively charged amino acids are indicated in blue, negatively charged amino acids in orange, polar in light blue, nonpolar in green, and Pisystem-dependent Pi stacking interactions within in dark green, and purple arrows indicate hydrogen bonds.

Table 3. *In vitro* Anti-*Plasmodial* Activity against the *P. falciparum* N54 Strain and Cytotoxicity toward Cells Chinese Hamster Ovarian (CHO) and Hepatocellular Carcinoma (HepG2)[a]

compound	PfN54 IC_{50} (μM)	CHO IC_{50} (μM)	CHO SI	HepG2 IC_{50} (μM)	HepG2 SI	solubility at pH 6.5 (μM)
FM1	2.80 ± 0.95	32.88	11.7	40.25	14.38	80
FM2	0.14 ± 0.04	>50	>357	>50	>357	80
FM4	0.92 ± 0.11	>50	>54	6.98	>8	<5
FM6	1.76 ± 0.29	>50	>28	12.82	7	<5
FM5	1.97 ± 0.44	>50	>25	0.84	0	80
F10	3.86 ± 2.14	>50	>13	>50	>13	ND
F12	4.50 ± 1.50	>50	>11	>50	>11	ND
F11	6.00 ± n/a	>50	>8	>50	>8	ND

[a]ND = not determined.

https://doi.org/10.1021/acsomega.3c04494
ACS Omega 2023, 8, 38220−38232

Table 4. Binding Affinities and % Inhibition of PfHsp90 and Human Hsp90[a]

compounds	FP inhibition % PfHsp90 [10 μM]	FP inhibition% human Hsp90 [10 μM]	K_a (1/Ms)($\times 10^3$)	K_d (1/s)($\times 10^{-6}$)	K_D (μM)
FM1	48 ± 3.8	23 ± 8.5	ND	ND	ND
FM2	69 ± 0.5	no inhibition	9.53 ± 1.54	1.26 ± 9.5	13.5 ± 2.2
FM4	32 ± 2.6	no inhibition	95.3 ± 88.2	8.57 ± 9.2	2.45 ± 0.0
FM6	25 ± 5.3	no inhibition	0.48 ± 0.10	102 ± 2.7	0.21 ± 0.0
F10	97 ± 7.9	44 ± 10.3	ND	ND	ND
F11	93 ± 10.8	38 ± 3.0	0.165 ± 0.45	584 ± 334	3.35 ± 1.5
harmine	7.0 ± 6.0	no inhibition	17.6 ± 14.9	3.20 ± 4.8	1.82 ± 0.1

[a]SPR data for the sensorgrams were generated to study the binding affinity of the compounds toward PfHsp90.

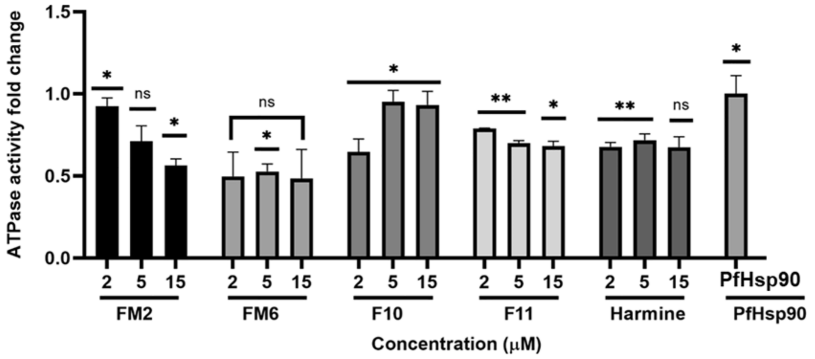

Figure 6. Compounds **FM2**, **FM6**, **F10**, and **F11** inhibit the intrinsic ATPase activity of PfHsp90. The effect of study compounds on the basal ATPase of PfHsp90 was investigated. Released Pi was monitored at 600 nm using a direct colorimetric assay.

ATPase Assays. The basal ATPase activity of PfHsp90 was determined using saturating levels of 2 mM ATP as previously reported[21] and varying concentrations (0.25−15 μM) of **FM2**, **FM6**, **F10**, and **F11**. harmine was used as a positive control for inhibition. We observed a decrease in the ATPase activity of PfHsp90 with an increase in the concentration of inhibition (Figure 6). The dose-dependent effect of the compounds was comparable to that of harmine (Figure 6). Since recombinant PfHsp90-NTD was used to conduct the assay, it is possible that the decrease in the ATPase activity of the chaperone suggests that the compounds bind at the same pocket as ATP as was suggested by molecular docking in this study.

CONCLUSIONS

The parasite *P. falciparum* is becoming increasingly resistant to the existing therapeutic drugs, making malaria a significant health issue.[1] A key focus of the WHO is the development of novel therapeutics, not only just for eradicating disease but also for addressing the growing problem of drug resistance against existing antimalarial agents.[1,2] To combat the drug resistance challenge, it is essential to explore validated drug targets, which will pave the way for the development of novel antimalarial drugs and counteract the rise of resistance. Notably, PfHsp90 stands out as a promising drug target of *P. falciparum*. The essential role of PfHsp90, a validated target, has been well established in the elimination of the *P. falciparum* parasite during the blood stage and liver stage.[25,52] Inhibition of PfHsp90 not only blocks the parasite's life cycle at the red blood cell stage but also leads to the clearance of parasitemia in the mouse model.[21] These findings underscore the pivotal significance of PfHsp90 in facilitating the progression of parasites through its various stages.

The present study sought to discover selective inhibitors that bind in the ATP binding pocket of PfHsp90 and inhibit its hydrolysis, consequently abrogating the function of PfHsp90. The study presents the generation of a pharmacophore model, DHHRR_1, which demonstrated the ability to identify novel potential inhibitors of PfHsp90 through screening of a compound library database. The DHHRR_1 model was used to conduct a virtual screening protocol, coupled with subsequent molecular docking studies utilizing both PfHsp90 and human Hsp90 receptors, facilitating the discovery of four top scoring compounds, representing the most promising binders among the total of 20 potential inhibitors of PfHsp90. The main drawback of molecular docking is the inability to account for water molecules for the effects of waters in binding affinity estimations and ligand strain energy caused by the binding event. In addition, our cross-docking suggests that GlideSP was system-dependent.

Therefore, to validate the in silico findings, a series of cell-based, biochemical, and biophysical assays were conducted. *In vitro* profiling of the compounds against *P. falciparum* revealed eight promising hits, showing a safety profile against mammalian cells. The compounds exhibiting anti-*Plasmodium* activity were evaluated for their ability to inhibit PfHsp90 using the ATPase, SPR, and FP assays. Biophysical assays revealed that compound **FM6** exhibited tight binding toward PfHsp90, indicated by a binding affinity (K_D) in the low micromolar range, while **FM2** bound to PfHsp90 with weak affinity as indicated by a binding affinity (K_D) higher than 10 μM.

The data from FPA showed that both compounds did not bind human Hsp90. **FM6** exhibited moderate activity against the *P. falciparum* NF54 strain. Moreover, taken together with the cytotoxicity data, where **FM6** was shown to be toxic to HepG2 cells and not CHO, we estimate that it is probable that this compound binds human Hsp90 beta (more active in cancer) than constitutive Hsp90. The weak binding affinity of **FM2** toward PfHsp90 contradicts its active *P. falciparum*NF54 potency, and we suggest that the compound might bind

https://doi.org/10.1021/acsomega.3c04494
ACS Omega 2023, 8, 38220−38232

nonspecifically to PfHsp90. The data obtained for **FM2** is not surprising as farnesyltransferase has been suggested as a target for the compound.[53] Like **FM6**, cysteine proteases have been suggested as a target for the compound.[54] While it is acknowledged that the major limitation of our study was that the pharmacophore model we used was trained using whole-cell activity data and not enzyme IC_{50}, the binding affinity data from SPR suggest tight binding between **FM6** and PfHsp90. Thus, the possibility of dual inhibition, which would offer advantages, including improved efficacy across the parasite life cycle, by **FM2** and **FM6** cannot be ruled out. Future studies could include other biophysical techniques (X-ray crystallography, nuclear magnetic resonance, and Cryo-EM) to further elucidate the compounds' mode of action toward the target. Immunoprecipitation assays would be desirable to assess whether the compounds are dual inhibitors.

Overall, promising results were obtained for compounds **F10** and **F11** as selective inhibitors of PfHsp90, despite their moderate whole-cell potency toward the *P. falciparum* NF54 strain. We found that these compounds disrupted the activity of PfHsp90 and were more selective to PfHsp90 than human Hsp90. Compound **FM4** was toxic toward the HepG2 cells, manifesting active activity toward *P. falciparum* NF54. Future studies could expand on these compounds to explore their structure−activity relationship with PfHsp90 for optimization efforts to improve their selectivity, potency, and affinity.

■ ASSOCIATED CONTENT

Supporting Information

The Supporting Information is available free of charge at https://pubs.acs.org/doi/10.1021/acsomega.3c04494.

Chemical structures of 31 selective inhibitors of PfHsp90 and the 20 potential hit compounds (Table S1 and Figure S1). Cross-docking (Figures S2 and S3). Induced fit docking for the other potential hit compounds toward PfHsp90 (Figure S4). Docking pose toward human Hsp90 (Figures S5 and S6). Anti-*Plasmodial* and cytotoxicity of the compounds (Table S2). PfHsp90-NTD and human Hsp90-NTD purifications (Figure S7). Binding assay (Figure S8). Binding affinity (Figure S9) (PDF)

■ AUTHOR INFORMATION

Corresponding Author

Fortunate Mokoena − *Department of Biochemistry, North-West University, Mmabatho 2735, South Africa;* orcid.org/0000-0003-0864-9157; Email: Fortunate.Mokoena@nwu.ac.za

Authors

Ofentse Mafethe − *Department of Biochemistry, North-West University, Mmabatho 2735, South Africa*

Tlhalefo Ntseane − *Department of Biochemistry, North-West University, Mmabatho 2735, South Africa*

Tendamudzimu Harmfree Dongola − *Department of Biochemistry and Microbiology, University of Venda, Thohoyandou 0950, South Africa*

Addmore Shonhai − *Department of Biochemistry and Microbiology, University of Venda, Thohoyandou 0950, South Africa*

Njabulo Joyfull Gumede − *Department of Chemical and Physical Sciences, Faculty of Natural Sciences, Walter Sisulu University (WSU), Umthatha, Eastern Cape 4099, South Africa;* orcid.org/0000-0003-4213-5416

Complete contact information is available at: https://pubs.acs.org/10.1021/acsomega.3c04494

Notes

The authors declare no competing financial interest.

■ ACKNOWLEDGMENTS

The financial contribution of the Grand Challenges Africa Drug Discovery Seed Grant (GCA/Round10/DD-065) is hereby acknowledged. We also acknowledged the Centre for High Performance Computing (CHPC) for access to Schrodinger's suite. The cell-based assays against the *P. falciparum* NF54 strain and cytotoxicity using mammalian Chinese hamster ovarian (CHO) and hepatocellular carcinoma cell lines and solubility were conducted at the University of Cape Town by Holistic Drug Discovery and Development (H3D).

■ REFERENCES

(1) World Health Organization. *World Malaria Report*. Vol. *WHO/HTM/GM*; World Health Organization. 2021. 238 p.

(2) Report WM. *World malaria report*; World Health Organization 2020, 2020.

(3) Siddiqui, F. A.; Liang, X.; Cui, L. Plasmodium falciparum resistance to ACTs: Emergence, mechanisms, and outlook. *Int. J. Parasitol Drugs drug Resist.* **2021**, *16*, 102−118.

(4) Dhorda, M.; Amaratunga, C.; Dondorp, A. M. Artemisinin and multidrug-resistant Plasmodium falciparum - a threat for malaria control and elimination. *Curr. Opin Infect Dis.* **2021**, *34* (5), 432−439.

(5) White, N. J. Antimalarial drug resistance. *J. Clin Invest.* **2004**, *113* (8), 1084−1092.

(6) Ocan, M.; Akena, D.; Nsobya, S.; Kamya, M. R.; Senono, R.; Kinengyere, A. A.; et al. Persistence of chloroquine resistance alleles in malaria endemic countries: a systematic review of burden and risk factors. *Malar. J.* **2019**, *18* (1), 76.

(7) Uwimana, A.; Legrand, E.; Stokes, B. H.; Ndikumana, J-LM; Warsame, M.; Umulisa, N.; et al. Emergence and clonal expansion of in vitro artemisinin-resistant Plasmodium falciparum kelch13 R561H mutant parasites in Rwanda. *Nat. Med.* **2020**, *26* (10), 1602−1608.

(8) Ashley, E. A.; Dhorda, M.; Fairhurst, R. M.; Amaratunga, C.; Lim, P.; Suon, S.; et al. Spread of artemisinin resistance in Plasmodium falciparum malaria. *N. Engl. J. Med.* **2014**, *371* (5), 411−423.

(9) Shahinas, D.; Folefoc, A.; Taldone, T.; Chiosis, G.; Crandall, I.; Pillai, D. R. A purine analog synergizes with chloroquine (CQ) by targeting Plasmodium falciparum Hsp90 (PfHsp90). *PLoS One.* **2013**, *8* (9), No. e75446.

(10) Corey, V. C.; Lukens, A. K.; Istvan, E. S.; Lee, M. C. S.; Franco, V.; Magistrado, P.; et al. A broad analysis of resistance development in the malaria parasite. *Nat. Commun.* **2016**, *7* (1), 11901.

(11) Hartl, F. U.; Bracher, A.; Hayer-Hartl, M. Molecular chaperones in protein folding and proteostasis. *Nature* **2011**, *475* (7356), 324−332.

(12) Gitau, G. W.; Mandal, P.; Blatch, G. L.; Przyborski, J.; Shonhai, A. Characterisation of the Plasmodium falciparum Hsp70-Hsp90 organising protein (PfHop). *Cell Stress Chaperones.* **2012**, *17* (2), 191−202.

(13) Banumathy, G.; Singh, V.; Pavithra, S. R.; Tatu, U. Heat Shock Protein 90 Function Is Essential for Plasmodium falciparum Growth in Human Erythrocytes*. *J. Biol. Chem.* **2003**, *278* (20), 18336−18345.

(14) Kumar, R.; Musiyenko, A.; Barik, S. The heat shock protein 90 of Plasmodium falciparum and antimalarial activity of its inhibitor, geldanamycin. *Malar. J.* **2003**, *2*, 30.

(15) Neckers, L.; Ivy, S. P. Heat shock protein 90. *Curr. Opin Oncol.* **2003**, *15* (6), 419−424.
(16) Whitesell, L.; Lin, N. U. HSP90 as a platform for the assembly of more effective cancer chemotherapy. *Biochim. Biophys. Acta* **2012**, *1823* (3), 756−766.
(17) Neckers, L.; Workman, P. Hsp90 molecular chaperone inhibitors: are we there yet? *Clin cancer Res. an Off J. Am. Assoc Cancer Res.* **2012**, *18* (1), 64−76.
(18) Jhaveri, K.; Taldone, T.; Modi, S.; Chiosis, G. Advances in the clinical development of heat shock protein 90 (Hsp90) inhibitors in cancers. *Biochim. Biophys. Acta* **2012**, *1823* (3), 742−755.
(19) Yu, J.; Zhang, C.; Song, C. Pan- and isoform-specific inhibition of Hsp90: Design strategy and recent advances. *Eur. J. Med. Chem.* **2022**, *238*, No. 114516.
(20) Hoy, S. M. Pimitespib: First Approval. *Drugs.* **2022**, *82* (13), 1413−1418.
(21) Pallavi, R.; Roy, R.; Reddy, R.; Venketesh, S.; Kumar, R.; Gupta, A. K. Heat Shock Protein 90 as a Drug Target against Protozoan Infections BIOCHEMICAL CHARACTERIZATION OF HSP90 FROM Plasmodium falciparum AND TRYPANOSOMA EVANSI AND EVALUATION OF ITS INHIBITOR AS A CANDIDATE DRUG. *J. Biol. Chem.* **2010**, *285* (49), 37964−37975.
(22) Pick, E.; Kluger, Y.; Giltnane, J. M.; Moeder, C.; Camp, R. L.; Rimm, D. L. High HSP90 expression is associated with decreased survival in breast cancer. *Cancer Res.* **2007**, *67* (7), 2932−2937.
(23) Que, N. L. S.; Crowley, V. M.; Duerfeldt, A. S.; Zhao, J.; Kent, C. N.; Blagg, B. S. J. Structure Based Design of a Grp94-Selective Inhibitor: Exploiting a Key Residue in Grp94 To Optimize Paralog-Selective Binding. *J. Med. Chem.* **2018**, *61* (7), 2793−2805.
(24) Trepel, J.; Mollapour, M.; Giaccone, G.; Neckers, L. Targeting the dynamic HSP90 complex in cancer. *Nat. Rev. Cancer* **2010**, *10* (8), 537−549.
(25) Posfai, D., Eubanks, A. L., Keim, A. I., Lu, K.-Y., Wang, G. Z., Hughes, P. F., et al. Identification of Hsp90 Inhibitors with Anti-Plasmodium Activity. *Antimicrob. Agents Chemother.* **2018** ;*62* (4) 10.
(26) Corbett, K. D.; Berger, J. M. Structure of the ATP-binding domain of Plasmodium falciparum Hsp90. *Proteins.* **2010**, *78* (13), 2738−2744.
(27) Wang, T.; Bisson, W. H.; Mäser, P.; Scapozza, L.; Picard, D. Differences in conformational dynamics between Plasmodium falciparum and human Hsp90 orthologues enable the structure-based discovery of pathogen-selective inhibitors. *J. Med. Chem.* **2014**, *57* (6), 2524−2535.
(28) Shahinas, D.; Macmullin, G.; Benedict, C.; Crandall, I.; Pillai, D. R. harmine is a potent antimalarial targeting Hsp90 and synergizes with chloroquine and artemisinin. *Antimicrob. Agents Chemother.* **2012**, *56* (8), 4207−4213.
(29) Wang, T.; Mäser, P.; Picard, D. Inhibition of Plasmodium falciparum Hsp90 Contributes to the Antimalarial Activities of Aminoalcohol-carbazoles. *J. Med. Chem.* **2016**, *59* (13), 6344−6352.
(30) Everson, N.; Bach, J.; Hammill, J. T.; Falade, M. O.; Rice, A. L.; Guy, R. K.; et al. Identification of Plasmodium falciparum heat shock 90 inhibitors via molecular docking. *Bioorg Med. Chem. Lett.* **2021**, *35*, No. 127818.
(31) Schrödinger Release 2021−3. *Protein Preparation Wizard; Epik, Schrödinger, LLC: New York, NY*. Impact, Schrödinger. 2021; Prime, Sch (New York, NY): LLC, 2021.
(32) Schrödinger Release 2021−2. *Maestro. Maestro. 2021*; Schrödinge (LLC): New York, NY.
(33) Obermann, W. M.; Sondermann, H.; Russo, A. A.; Pavletich, N. P.; Hartl, F. U. In vivo function of Hsp90 is dependent on ATP binding and ATP hydrolysis. *J. Cell Biol.* **1998**, *143* (4), 901−910.
(34) Schrödinger Release 2021−2. *MacroModel. Schrödinger*. 2021; LLC: New York, NY.
(35) Schrödinger Release 2021−3. *LigPrep. LigPrep*. 2021; Schrödinge (LLC): New York, NY.
(36) Jorgensen, W. L.; Maxwell, D. S.; Tirado-Rives, J. Development and Testing of the OPLS All-Atom Force Field on Conformational Energetics and Properties of Organic Liquids. *J. Am. Chem. Soc.* **1996**, *118* (45), 11225−11236.
(37) Schrödinger Release 2021−2. *Phase. Schrödinger. 2021*; LLC: New York, NY.
(38) Zou, K. H.; O'Malley, A. J.; Mauri, L. Receiver-operating characteristic analysis for evaluating diagnostic tests and predictive models. *Circulation.* **2007**, *115* (5), 654−657.
(39) Giménez, B. G.; Santos, M. S.; Ferrarini, M.; Fernandes, J. P. S. Evaluation of blockbuster drugs under the rule-of-five. *Pharmazie.* **2010**, *65* (2), 148−152.
(40) Schrödinger Release 2021−2. *Glide. Schrödinger. 2021*; LLC: New York, NY.
(41) Wang, H.; Aslanian, R.; Madison, V. S. Induced-fit docking of Mometasone furoate and further evidence for glucocorticoid receptor 17α pocket flexibility. *J. Mol. Graph Model.* **2008**, *27* (4), 512−521.
(42) Prime. Schrödinger Release 2021−2. *Schrödinger. 2021*; LLC New York: NY.
(43) Li, J.; Abel, R.; Zhu, K.; Cao, Y.; Zhao, S.; Friesner, R. A. The VSGB 2.0 model: a next generation energy model for high resolution protein structure modeling. *Proteins* **2011**, *79* (10), 2794−2812.
(44) Makler, M. T.; Ries, J. M.; Williams, J. A.; Bancroft, J. E.; Piper, R. C.; Gibbins, B. L.; et al. Parasite lactate dehydrogenase as an assay for Plasmodium falciparum drug sensitivity. *Am. J. Trop Med. Hyg.* **1993**, *48* (6), 739−741.
(45) Mosmann, T. Rapid colorimetric assay for cellular growth and survival: application to proliferation and cytotoxicity assays. *J. Immunol. Methods.* **1983**, *65* (1−2), 55−63.
(46) Silva, N. S. M.; Bertolino-Reis, D. E.; Dores-Silva, P. R.; Anneta, F. B.; Seraphim, T. V.; Barbosa, L. R. S.; et al. Structural studies of the Hsp70/Hsp90 organizing protein of Plasmodium falciparum and its modulation of Hsp70 and Hsp90 ATPase activities. *Biochim. Biophys. Acta Proteins Proteomics.* **2020**, *1868* (1), No. 140282.
(47) Matambo, T. S.; Odunuga, O. O.; Boshoff, A.; Blatch, G. L. Overproduction, purification, and characterization of the Plasmodium falciparum heat shock protein 70. *Protein Expr. Purif.* **2004**, *33* (2), 214−222.
(48) Lebepe, C. M.; Matambanadzo, P. R.; Makhoba, X. H.; Achilonu, I.; Zininga, T.; Shonhai, A. Comparative Characterization of Plasmodium falciparum Hsp70−1 Relative to E. coli DnaK Reveals the Functional Specificity of the Parasite Chaperone. *Biomolecules* **2020**, *10* (6), 856 DOI: 10.3390/biom10060856.
(49) Muthelo, T.; Mulaudzi, V.; Netshishivhe, M.; Dongola, T. H.; Kok, M.; Makumire, S.; et al. Inhibition of Plasmodium falciparum Hsp70-Hop partnership by 2-phenylthynesulfonamide. *Front Mol. Biosci.* **2022**, *9*, No. 947203.
(50) Taminau, J.; Thijs, G.; De Winter, H. Pharao: pharmacophore alignment and optimization. *J. Mol. Graph Model.* **2008**, *27* (2), 161−169.
(51) Carter, J. V.; Pan, J.; Rai, S. N.; Galandiuk, S. ROC-ing along: Evaluation and interpretation of receiver operating characteristic curves. *Surgery* **2016**, *159* (6), 1638−1645.
(52) Banumathy, G.; Singh, V.; Pavithra, S. R.; Tatu, U. Heat Shock Protein 90 Function Is Essential for Plasmodium falciparum Growth in Human Erythrocytes. *Biochemistry* **2003**, *278* (20), 18336−18345.
(53) Cowell, A. N.; Istvan, E. S.; Lukens, A. K.; Gomez-Lorenzo, M. G.; Vanaerschot, M.; Sakata-Kato, T. Mapping the malaria parasite druggable genome by using in vitro evolution and chemogenomics. *Science* **2018**, *359* (6372), 191−199.
(54) Pereira, G. A. N.; da Silva, E. B.; Braga, S. F. P.; Leite, P. G.; Martins, L. C.; Vieira, R. P. Discovery and characterization of trypanocidal cysteine protease inhibitors from the "malaria box. *Eur. J. Med. Chem.* **2019**, *179*, 765−778.
(55) Llauger-Bufi, L.; Felts, S. J.; Huezo, H.; Rosen, N.; Chiosis, G. Synthesis of novel fluorescent probes for the molecular chaperone Hsp90. *Bioorg. Med. Chem. Lett.* **2003**, *13* (22), 3975−3978.
(56) Mobley, D. L.; Dill, K. A. Binding of Small-Molecule Ligands to Proteins: "What you See" Is Not Always "What you Get". *Structure* **2009**, *17*, 489−498.

(57) Zhou, Z.; Felts, A. K.; Friesner, R. A.; Levy, R. M. Comparative performance of several flexible docking programs and scoring functions: enrichment studies for a diverse set of pharmaceutically relevant targets. *J. Chem. Inf. Model.* **2007**, *47*, 1599−1608.
(58) Warren, G. L.; Andrews, C. W.; Capelli, A.-M.; Clarke, B.; LaLonde, J.; Lambert, M. H.; Lindvall, M.; Nevins, N.; Semus, S. F.; Senger, S.; Tedesco, G.; Wall, I. D.; Woolven, J. M.; Peishoff, C. E.; Head, M. S. A critical Assessment of Docking Programs and Scoring Functions. *J. Med. Chem.* **2006**, *49*, 5912−5931.
(59) Englebienne, P.; Fiaux, H.; Kuntz, D. A.; Corbeil, C. R.; Gerber-Lemaire, S.; Rose, D. R.; Moitessier, N. Evaluation of docking programs for predicting binding Golgi alpha-mannosidase ii inhibitors: a comparison with crystallography. *Proteins. Struct. Funct. Bioinf.* **2007**, *69*, 160−176.
(60) Tame, J. R. Scoring functions: a view from the bench. *J. Comp. Aided. Mol. Des.* **1999**, *13*, 99−108.

NOTE ADDED AFTER ASAP PUBLICATION

This paper originally published ASAP on September 26, 2023. Several references were missing, and a new version reposted on October 5, 2023.

https://doi.org/10.1021/acsomega.3c04494
ACS Omega 2023, 8, 38220−38232